Applied Catalysis B: Environmental 154–155 (2014) 301–308

Contents lists available at ScienceDirect

Applied Catalysis B: Environmental

journal homepage: www.elsevier.com/locate/apcatb

Photocatalytic degradation of butanone (methylethylketone) in a small-size TiO_2/β-SiC alveolar foam LED reactor

Nizar Doss, Pierre Bernhardt, Thierry Romero, Romain Masson, Valérie Keller, Nicolas Keller*

Institut de Chimie et Procédés pour l'Energie, l'Environnement et la Santé (ICPEES), CNRS, Strasbourg University, rue Becquerel, Strasbourg, France

ARTICLE INFO

Article history:
Received 12 August 2013
Received in revised form 15 February 2014
Accepted 19 February 2014
Available online 28 February 2014

Keywords:
LED
Photocatalysis
Titanium dioxide
Solid alveolar foams
Energy effectiveness

ABSTRACT

The feasibility of using Light Emitting Diodes (LEDs) as irradiation light source instead of usual conventional UV-A fluorescent light tube has been investigated for designing greener and small-size photocatalytic device for air purifying treatment. LEDs benefit from a high electricity-to-light yield, from the absence of any mercury, from strength and long lifetime, from the use of direct current power source and from an almost complete recycling. It was evidenced that the LED emission wavelengths need to carefully match with the absorption range of the photocatalyst, so that the use of widespread UV/vis 392 nm emission wavelength LEDs required its association with visible-light responsive TiO_2 MPT623 from ISK in place of TiO_2 P25. Thus, taking the gas phase methylethylketone degradation as test reaction, tests performed in a single-pass flow mode and in recirculation evidenced that the matching of UV/vis 392 nm emission wavelength LEDs to TiO_2 MPT623 was promising. It allowed, without any loss of performances, engineering a 133 cm^3 small-size 56 LED photoreactor – interesting notably in terms of system miniaturization and configuration flexibility -, in which a medium surface area open-cell β-SiC alveolar foam was used as structured photocatalyst support for TiO_2. The results illustrated the interest of using a supporting solid alveolar foam and small-size UV/vis LEDs adapted to the TiO_2 photocatalyst absorption range. TiO_2 MPT623/LEDs systems displayed energy effectiveness coefficients of about 50 times higher than that of TiO_2 P25/UV-A system, so that they could be considered as a valuable alternative in the search for energy saving technologies.

1. Introduction

The removal of airborne chemical pollutants from air is a challenging task for which oxidative photocatalysis has attracted a considerably growing attention for acting as an efficient air treatment technology because of the oxidizing power of UVA-irradiated semiconductors [1–3]. In parallel to other applications like self-cleaning surfaces or water purification, air remediation is thus a promising field of applications for photocatalysis from both preventive and curative points of view.

Compared to works devoted to the design of efficient photocatalytic materials and photoreactors, studies on alternatives to conventional fluorescent lamps as artificial light sources remain scarce. However, the widespread use of mercury-containing radiation sources associated to cost and energy consumption aspects are considered as bottlenecks for successfully implementing photocatalysis and designing efficient air treatment processes in the frame of a sustainable development approach. Works have been performed on optic fibers acting as light distributing guide [4–8], and now photocatalysis is envisaging benefiting from rapid and continuous progresses on high output inexpensive light emitting diodes (LEDs) for designing LED-based photoreactors for air treatment. The advantages shown by the LED alternative to conventional fluorescent lamps, are a small size (interesting notably in terms of system miniaturization and configuration flexibility), a long lifetime associated to the LED strength, a high electricity-to-light yield with little heating and a low energy consumption, the use of direct current power compared to alternative one, and the fact of being a "greener" mercury-free radiation source, with an almost complete recycling. Nowadays LEDs are emerging as a promising photochemical light source for remediation [9–16] and it is thus of interest to further evaluate the potential of LEDs as irradiation light source for photocatalytic purposes. They will benefit from a democratization in the forthcoming decades, drawing the planned evolution

* Corresponding author. Tel.: +33 0 368852811; fax: +33 0 368852761.
E-mail address: nkeller@unistra.fr (N. Keller).

http://dx.doi.org/10.1016/j.apcatb.2014.02.036
0926-3373/

perspectives of the LED market, with its progressive turn from specialty niches to a broader adoption and finally an expected fully democratized use at low costs.

The feasibility of applying LEDs instead of traditional fluorescent UV lamps for removing liquid and gas phase organics by photocatalysis has been explored, taking Reactive Red 22 and *o*-cresol, and formaldehyde as liquid and gas phase model compounds, respectively [9–11]. Shie et al. calculated an energy effectiveness coefficient for UV light sources, largely in favor of UV LEDs, being 131 and 99 times greater than for UV-C and UV-A lamps, respectively [11]. However, UV LEDs still suffer from low irradiance at adequate wavelengths or from cost limitations in the case of high irradiance LEDs. Therefore, works have been mainly performed with cheaper and more intense visible LEDs, thus requiring the use of visible light responsive modified-TiO_2 photocatalysts. The use of nanoporous silicon in UV LED- and green LED-powdered reactors for the diphenylbenzofuran photooxidation has been performed by Lapkin et al. [12], and in the field of TiO_2-based photocatalysts, Ghosh et al. compared the photocatalytic activity of TiO_2 P25 and tin-doped TiO_2 nanofibers under 350 nm UV light irradiation and that of coumarin C-343 dye coated TiO_2 nanofibers with 436 nm visible LEDs. Although TiO_2 P25 remained more efficient, they showed that the activity of C-343 coated TiO_2 nanofibers in the LED reactor was well competitive for the degradation of 4-chlorophenol in water [13,14]. Liu et al. studied the activity of S-doped TiO_2 under low power 460 nm visible LEDs for orange methyl removal [15]. N-doped TiO_2 hollow spheres synthesized by Subagio et al. benefited from high surface area, high porosity and low bulk density to enhance photonic efficiency and dispersivity in the LED reactor compared to powder TiO_2 in the liquid phase mineralization of bisphenol-A [16].

Thus, we aimed here at investigating the use of LEDs in the design of a photocatalytic module for air treatment incorporating medium surface area open-cell β-SiC alveolar foams as structured photocatalyst support. Alveolar foams allowed elaborating flow-through structured photoreactors maintaining a suitable light transmission to the reactor core, and benefiting from the static mixer role provided by the foam, from the gain of exposed surface resulting in an increased surface-to-reactor volume ratio, as well as from very low pressure drops, as previously reported [17–22]. Butanone (methylethylketone, MEK), a typical malodorous pollutant of dwelling house indoor air, was taken as gas phase model Volatile Organic Compound [23].

2. Experimental

2.1. Material preparation

Two well-known commercial reference TiO_2 have been used, anatase/rutile Aeroxide(c) TiO_2 P25 (50 m^2/g) from Evonik as well as TiO_2 MPT623 (60 m^2/g) from Ishihara Sangyo Kaisha. TiO_2 MPT623 is a visible light responsive Pt chloride-modified rutile TiO_2 photocatalyst already applied to practical indoor applications [24,25]. XRD pattern of TiO_2 MPT623 exhibited diffraction peaks corresponding to the rutile TiO_2, with the main peaks at 27.5°, 36.1° and 54.4° corresponding to (1 1 0), (1 0 1) and (211) planes, respectively (Fig. 1A) [26].

LEDs, purchased from Roithner Lasertechnik (Austria), have been used as light source and renamed here according to their measured emission maximum wavelength (Table 1, *e.g.* LED392 is the shortcut label for LEDs with a measured wavelength of maximum emission at 392 nm). Fig. 1B shows the LED emission spectral range in regards to the absorption range of TiO_2. The UV-A irradiance emitted by the LEDs were recorded using a wideband RPS900-W Rapid Portable Spectroradiometer from International Light

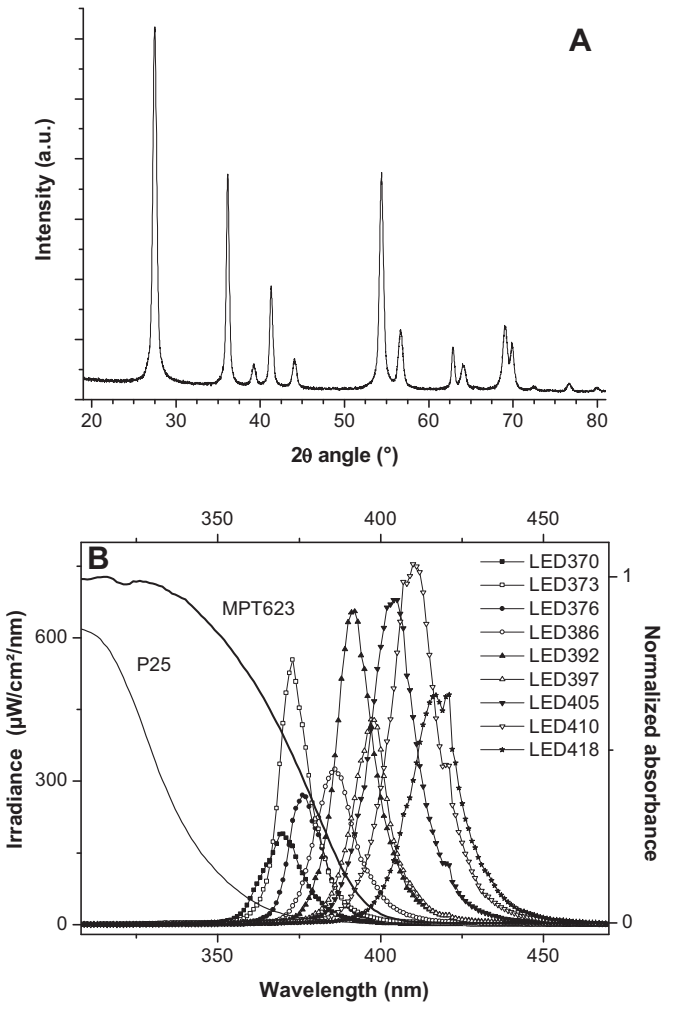

Fig. 1. (A) XRD pattern of TiO_2 MPT623; (B) LED emission spectral range and UV/vis absorption range of commercially available TiO_2 P25 and TiO_2 MPT623. The LEDs have been renamed according to the measured maximum emission wavelength.

Technology. Measurements were performed as closest as possible from a single LED and the LED geometry required averaging the irradiance data recorded for different locations at the LED surface.

Medium surface area open cell β-SiC alveolar foam was synthesized by the SICAT Company (Willstätt-Germany) according to the Shape Memory Synthesis replica method, in which a pre-shaped polyurethane foam is transformed into its corresponding carbide at 1360 °C under argon [27]. It reflects the fact that the original macrostructural features of a solid, *i.e.* its macroscopic shape, were retained after synthesis. Thus, β-SiC solid foam with a surface area of 20 m^2/g can be manufactured with different shapes for being adjusted to the photoreactor geometry and size. Fig. 2 shows a high degree of interconnectivity through the entire matrix of the foams. They could be successfully modeled by Edouard and coll [28] as the packing of regular pentagonal dodecahedron. The small thickness of the struts constituting the foams is beneficial to mass transfer properties. The most characteristic parameters of the β-SiC foam are the size of the cell (ϕ), the windows (or pore diameter (a)), which can be measured by several techniques and correlated to pore density (the number of pores per linear inch, ppi) as well as the struts diameter (ds). The alveolar foam parameters were measured by optical imaging at 5440 ± 720 μm, 2290 ± 630 μm and 575 ± 80 μm respectively, with 95–97% open porosity. The large average cell size of open cell β-SiC foam was previously reported to be beneficial to a suitable light penetration to the core of the

Table 1
Some characteristics of commercial LEDs. (*) and (**) correspond to measured data and technical data provided by the supplier, respectively. The UV-A irradiance values measured suffer from a non negligible uncertainty, as a result from the difficulty to record the irradiance close to the LED surface, notably due to the LED geometry that required averaging the irradiance data recorded for different locations at the LED surface.

Roithner Laser Technik LED References	Shortcut label	Measured wavelength of maximum emission (nm)* [supplier technical data, nm]**	Spectral band-width ($\Delta\lambda$, nm)*	Total measured irradiance (mW/cm^2)*	LED electrical power (mW, min-max)**
XSL-365-3E	LED370	370 [365]	14	2.2 ± 0.7	2.4–6.0
XSL-370-3E	LED372	372 [370]	12	2.5 ± 0.8	4.0–6.0
UVLED370-110E	LED376	376 [370]	12	3.9 ± 2.3	5.5
UVLED375-10-30	LED373	373 [375]	10	7.3 ± 1.5	10
LED385-04	LED386	386 [385]	14	6.4 ± 1.7	11
VL390-5-15	LED392	392 [390]	15	11.7 ± 2.0	8.1–11.5
RLU395-8-30	LED395	397 [395]	15	7.64 ± 1.3	8
VL400-5-15	LED405	405 [400]	16	12.0 ± 2.0	8.1–11.5
VL410-5-15	LED410	410 [410]	16	15.6 ± 2.2	10–16
VL415-5-15	LED418	418 [415]	18	10.6 ± 1.6	11.5–16.3

foam, that was modeled in a first approximation by a decreasing exponential as a function of foam thickness [22]. Characterization can be found in [19–22].

The deposition of TiO_2 MPT623 and P25 photocatalysts onto the alveolar β-SiC foam was performed by immerging the β-SiC foam support into a TiO_2-containing water suspension and further drying the sample at ambient temperature. The impregnation suspension, with TiO_2 concentration ranged from 100 to 200 g/L depending on the targeted TiO_2 amount to deposit, was kept under stirring for 30 min before turning off the stirring for immerging the foam. The impregnation process was replicated, with pressurized air flow treatment between each step, until the desired TiO_2 mass was obtained. The β-SiC foam coated TiO_2 material was weighted after a final drying at 100 °C and an ultrasonic treatment for determining the TiO_2 content. SEM images evidenced the uniformity of the TiO_2 coating on the foam (Fig. 2).

2.2. Photocatalytic tubular flow reactor

The screening in reactivity was performed in a 40 mm diameter tubular flow Pyrex reactor, incorporating a 20 mm length and 40 mm diameter β-SiC foam and LEDs, as schematized in Fig. 3A. Illumination was provided by a set of 7 LEDs, homogeneously distributed on a grid orthogonal to the flow, with an illuminated effective length of 20 mm, corresponding to the β-SiC foam thickness. In that case, 300 mg of TiO_2 photocatalyst was deposited on the β-SiC foam cylinder, corresponding to a TiO_2 content of 8.9 ± 0.2 wt.%. Methylethylketone (Sigma–Aldrich, >99%) and water were fed at ambient temperature and atmospheric pressure by bubbling air through two saturators respectively, and mixed with additional air to obtain a MEK concentration of 240 ppm_v and a relative humidity of 30% with a total flow of 500 mL/min. It corresponded to a gas velocity of 0.66 cm/s and a residence time of 3 s. Before the photocatalytic reaction, the catalyst was first exposed to the polluted air stream with no illumination until dark-adsorption equilibrium was reached, and afterwards illumination was switched on. The photocatalytic performances were obtained by *on-line* quantifying inlet and outlet flows with a micro-gaschromatography (Agilent μGC 3000A), equipped with high sensitivity modules containing thermal conductivity detectors as well as PoraPlotU, OV1 and Stabilwax columns allowing detection of MEK, water, CO_2 and organic byproducts such as acetaldehyde. Limits of detection/quantification are 0.1 ppm_v and 1 ppm_v for organic molecules and CO_2, respectively, and relative analytical uncertainty has been determined at 5%.

For approximate comparison, a UV-A fluorescent tube (Philips-TL4WBLB, 112 mm × 16 mm $l \times d$) with a spectral peak centered on 365 nm was used, axially located inside the tubular reactor, and with an irradiance of 3.1 mW/cm^2 received by the TiO_2 coating (Emission spectrum in Supporting Information S1). In that case,

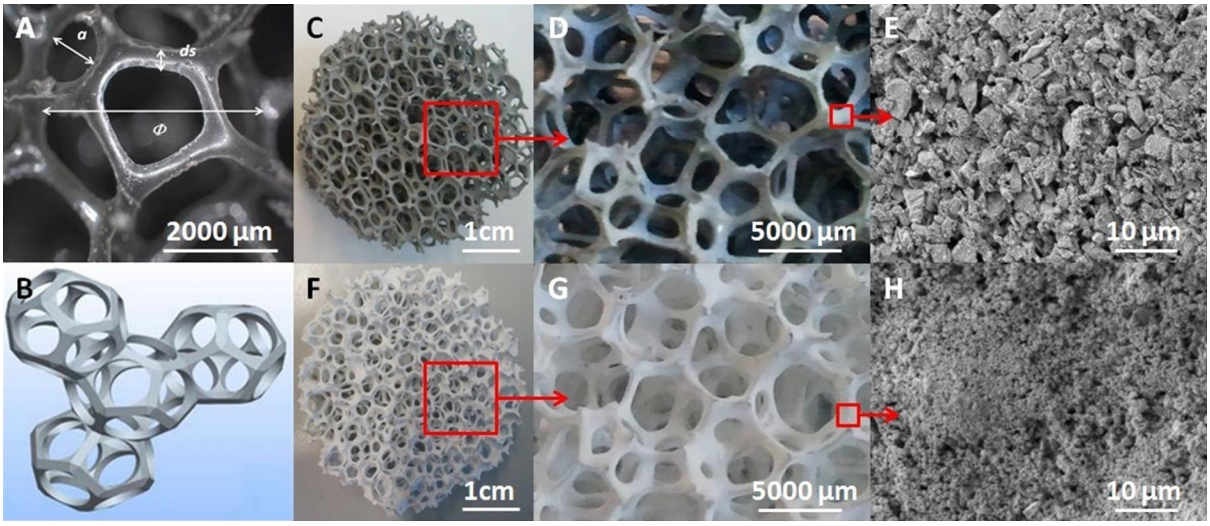

Fig. 2. (A) Precursor polyurethane foam image, evidencing the cell size (ϕ), the window size (a) and the strut diameter (ds) characteristics of the foam. (B) Schematic drawing of the model developed by Edouard, with packing of regular pentagonal dodecahedron, taken from [28]. (C–E) Optical and SEM images of the open cell β-SiC alveolar foam. (F–H) Optical and SEM images of the TiO_2 MPT623/β-SiC foam photocatalytic material.

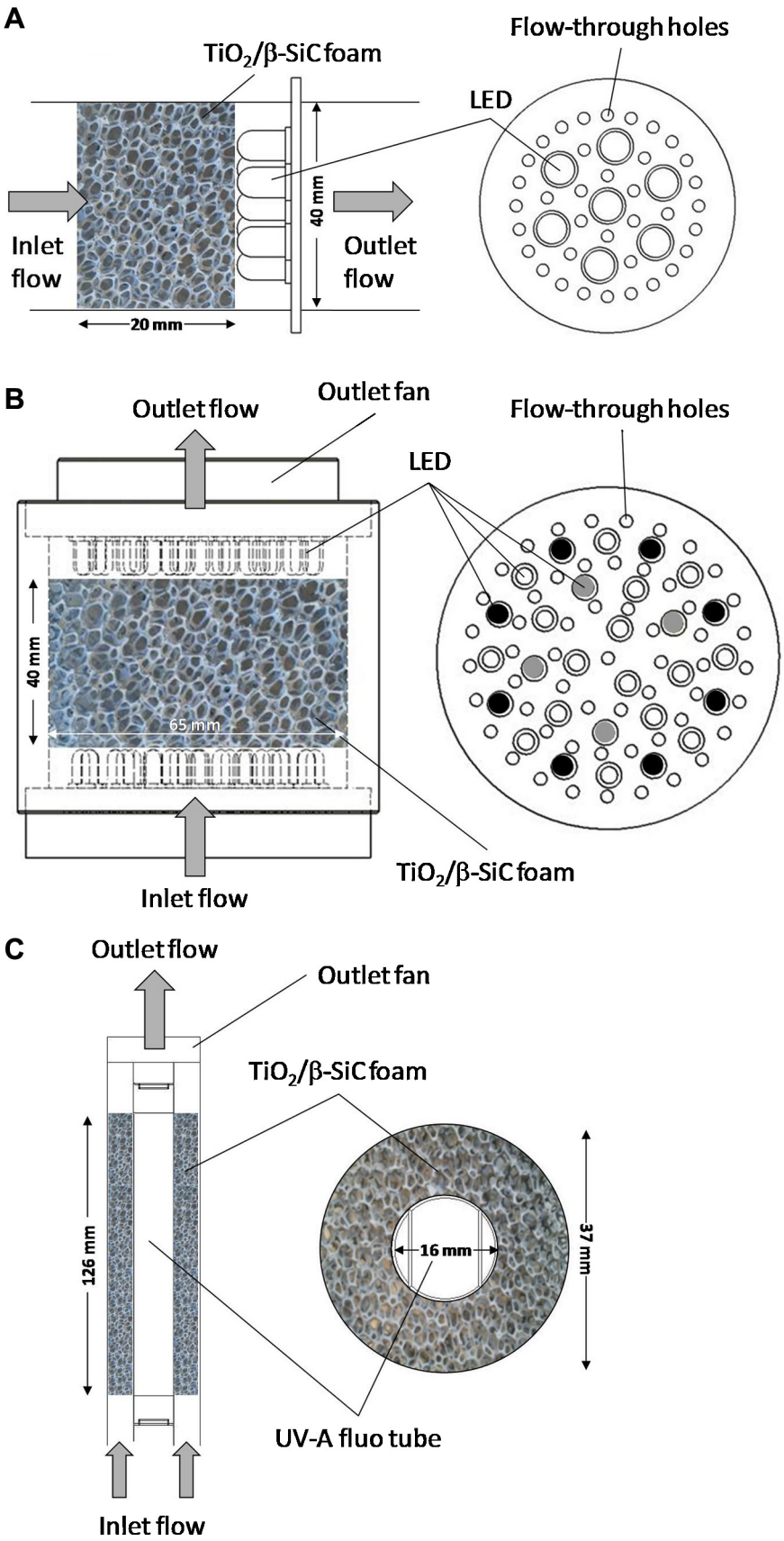

Fig. 3. (A) Scheme of the TiO_2 MPT623/β-SiC foam and LEDs – based single pass flow-through photocatalytic reactor used for screening in reactivity. (B) Scheme of the flow-through structured photocatalytic reactor incorporating LEDs and the TiO_2 MPT623/β-SiC foam. In addition to both top- and bottom-located LED printed circuit boards, it includes a 10 m^3/h inner fan for working in a recirculation mode inside the test chamber. In the 56 LED configuration, all the LEDs were lighted on (dark, gray and white), whereas only white and gray LEDs, and only gray LEDs were lighted on in 40 and 8 LED configurations, respectively. The LEDs were equally distributed between both top- and bottom-printed circuits. (C) Scheme of the flow-through photocatalytic reactor structured by the TiO_2 MPT623/β-SiC foam material and built around a conventional UV-A fluorescent tube.

by evaporating a photocatalyst containing aqueous suspension to dryness, 300 mg of photocatalyst was evenly coated over a 23 mm length on the internal surface of the tube (*i.e.* a 10.4 mg/cm^2 surface density), corresponding to the 'effective' length of the reactor, so that the test was performed at 500 mL/min total flow with an approximatively similar residence time of 2.9 s within the illuminated zone.

2.3. Closed chamber as batch reactor and photocatalytic module

A 110 cm × 110 cm × 165 cm ($l \times L \times h$) parallelepipedic-shaped test chamber was used as closed reactor, with an inner volume of 2 m^3 (Supporting Information S2). It was made of low adsorption chemically inert materials, and was directly connected to a micro-gaschromatography. A photocatalytic reactor has been engineered for incorporating 8, 40 or 56 visible LEDs and a 65 mm × 40 mm ($d \times h$) disk of 5440 μm mean cell size β-SiC foam supported TiO_2 MPT623 photocatalytic material, with a TiO_2 content of 9.2 ± 0.2 wt.%, corresponding to 1.6 g of TiO_2 (Fig. 3B). In addition to the LED printed circuit boards, it includes an inner fan working at 10 m^3/h and the total volume of the photocatalytic material of 133 mL led to run the tests with a residence time of 0.048 s.

For approximate comparison, a similar flow-through photocatalytic reactor was built, based on a 4 W UV-A fluorescent tube (Philips-TL4WBLB, 112 mm × 16 mm $l \times d$) with a spectral peak centered on 365 nm and emitting with an irradiance of 4.9 mW/cm^2, axially incorporated inside a TiO_2 P25 (9.0 ± 0.2 wt.%)/β-SiC foam ring, as shown in Fig. 3C.

After introduction inside the test chamber of 20 ppm_v of MEK with a serynge and further homogeneisation of the chamber for 3 min, the photocatalytic module was turned on both in terms of lighting and inner fan. Quantification was performed with the Agilent μGC 3000 A micro-gaschromatography by *on-line* sampling every 3 min.

The experimental degradation data were expressed following the Langmuir-Hinshelwood model for deriving the apparent kinetic rate constant, known to be a *non-true* constant, taking into account that for highly diluted samples, the reaction is essentially an apparent first-order reaction. Although criticized [29,30], this model remains suitable for comparing data and photocatalytic systems. For targeting a possible industrial application and evaluating the interest of using LEDs as light sources in terms of energy gain, the energy effectiveness (E_e) was calculated for systems working in recirculation, as adapted from Shie et al. [11], as follows:

$$\text{Energy effectiveness}(E_e, \text{mg kW}^{-1}\text{ h}^{-1}) = \frac{\text{degraded MEK mass (mg)}}{\text{input power (kW h)}} = \frac{(C_0 - C) \times 10^{-3} \times M}{p \times t} \times \frac{V}{V_M}$$

where C_0 is the initial MEK concentration (ppm_v), C the MEK concentration at time t (ppm_v), M the MEK molecular weight (g mol^{-1}), V the chamber volume (L), V_M the molar volume (L mol^{-1}), p the consumed energy power (kW) and t the reaction time (h).

3. Results and discussion

3.1. Single-pass tests

Fig. 4A shows the MEK conversion and the mineralization yield into CO_2 obtained in a single-pass mode over TiO_2 P25 and TiO_2 MPT623 photocatalysts for different irradiation wavelengths with LED373, LED392 and LED410 as LED light sources, for jointly investigating the influence of the TiO_2 photocatalyst nature and of the activation wavelength from UV to the beginning of the visible range. The TiO_2 P25 offered a superior efficiency in terms of both MEK removal and mineralization yield into CO_2 with the LED at

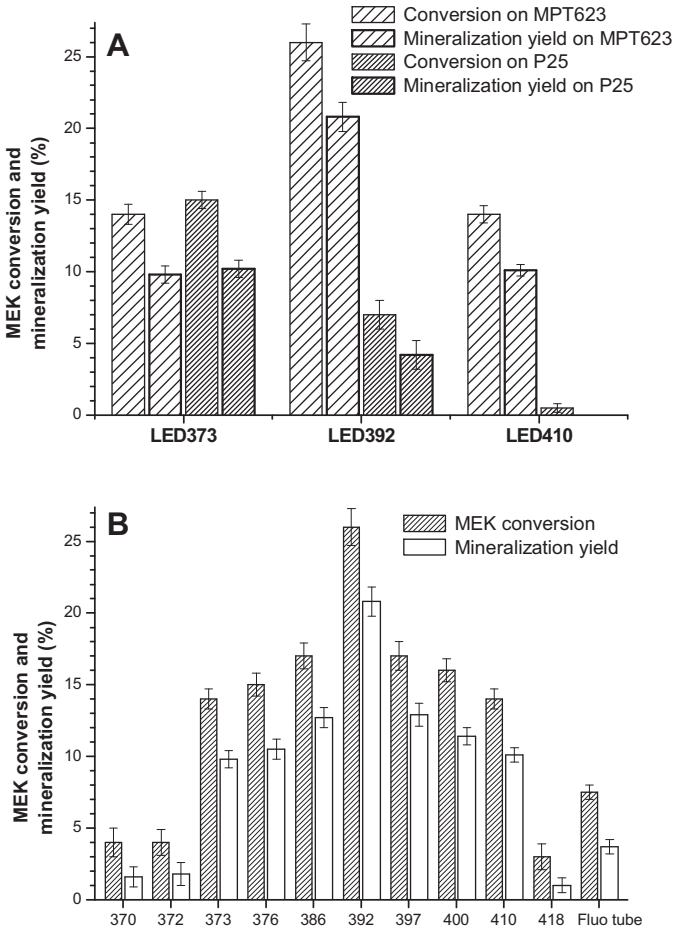

Fig. 4. MEK conversions and mineralization yield into CO_2 obtained in single-pass screening tests (A) over TiO_2 P25 and TiO_2 MPT623 photocatalysts supported at 8.9 ± 0.2 wt.% on the β-SiC alveolar foam for different irradiation wavelengths with LED373, LED392 and LED410 as LED light sources, and (B) over TiO_2 MPT623 (8.9 ± 0.2 wt.%)/β-SiC alveolar foam as a function of the LED light source.

373 nm, with a MEK conversion of 15% and mineralization yield into CO_2 of 10%. Whatever the photocatalyst and the irradiation source, acetaldehyde has also been detected as the main reaction intermediate in the photocatalytic oxidation of MEK, as expected [23]. The detection of acetaldehyde allowed to almost close the carbon mass balance, taking also into account some VOCs in negligible amounts, detected but neither identified nor quantified by the micro-gas chromatography.

Increasing the irradiation wavelength toward the beginning of the visible range pointed out the interest of using the TiO_2 MPT623 photocatalyst. Indeed, TiO_2 MPT623 led at 392 nm and at 410 nm to MEK conversions of 26% and 14% respectively, and mineralization yields into CO_2 of 21% and 10%, respectively, while the use of TiO_2 P25 resulted in similar conditions in low MEK conversions of 7% and 0.5% respectively, with mineralization yields of 4% and of a too low level to be quantified, respectively. This behavior resulted in a first approximation from the relationship between the TiO_2 absorption range and the LED emission wavelengths, shown in Fig. 1. At low wavelengths, suitable for TiO_2 P25, the photocatalyst displayed the highest MEK conversion and the highest mineralization yield, but the system suffered from the low irradiance of the UV-A LED373, whereas this reference TiO_2 was not appropriate for a higher wavelength irradiation. Since high irradiance LEDs with UV-A wavelengths adequate for TiO_2 P25 remained unacceptably highly expensive for targeting a real use for designing LEDs-based

air treatment devices, the TiO_2 MPT623 photocatalyst has been thus selected for further investigation.

As a result, the influence of the irradiation wavelength has been further studied on the TiO_2 MPT623 photocatalyst, by changing the LED light sources, as illustrated in Fig. 4B. Low wavelength LEDs at 370 nm and 372 nm led to very low MEK conversions of 4%, and very low mineralization yields of about 1.5%, probably mainly as a result from the low irradiance of the LEDs (Table 1). Secondary minor reason could be the mismatch between the band gap and the activation wavelengths, that are in visible light region and in the UV-A light region, respectively, as shown in Fig. 1B, and that could be probably responsible for an increased recombination rate. When increasing the activation wavelength, most of the LED sources yielded MEK conversions ranging from 14% to 17%, with mineralization yield ranging from 10% to 13%, except the intermediate UV/vis LED at 392 nm, for which a higher MEK conversion of 26% and a higher mineralization yield of 21% were recorded. Finally, a very low MEK conversion of 3% with a very low mineralization yield of 1% were observed for visible LEDs centered on 418 nm, which were not able to significantly activate the TiO_2 MPT623 photocatalyst. In comparison, the UV-A fluorescence tube at 365 nm resulted in a MEK conversion of 7.5% and a mineralization yield of about 4%. The volcano-shaped curves of both the MEK removal efficiency and the mineralization yield obtained during the screening in the single-pass reactor, showed that using the TiO_2 MPT623 photocatalyst required adapting the LED emission wavelength without losing in radiant power, since too high or too low wavelength LEDs as well as too low intensity LEDs led to lower efficiencies than when using intermediate UV–vis LEDs. In that purpose, among the tested systems, the use of the 392 nm UV–vis LEDs seems to be a good compromise for matching in terms of activation wavelength with the TiO_2 MPT623band gap whereas offering a good radiant power.

As a result from tests performed in the tubular flow reactor, and based on MEK removal efficiencies and mineralization yields, LEDs with maximum emission wavelengths at 386 nm, 392 nm and 397 nm, and with medium radiant power, have been selected as light sources of the β-SiC foam-based photocatalytic module, for carrying out tests in recirculation inside the chamber.

3.2. Closed chamber characterization

Experimental measurements of the MEK concentration as a function of time at different locations inside the chamber showed that homogenization occurred in the chamber volume within less than 1 min. Simulation of the velocity field inside the chamber, based on fluid mechanics Navier–Stokes equations and performed with the COMSOL software [31], confirmed the experimental result (Supporting Information S3). In a first approximation, considering that the chamber ceiling is the farthest location from the photocatalytic module for evaluating the maximum time required for air to pass through the fan, *i.e.* for homogenizing the chamber, the velocity distribution calculated at the ceiling section showed a speed limit of 0.0331 m/s at 1.6 m distance. The chamber homogenizing time was then roughly evaluated to be 50 s, in agreement with the experimental results.

3.3. Recirculation tests in the chamber

First, blank tests performed in the absence of photocatalytic module showed the stability of the MEK concentration at 20 ± 0.5 ppm_v for 1500 min of operation (not shown), so that it was not necessary to introduce any chamber leakage effect within the first-order apparent rate constant, similarly to results obtained by Kartheuser et al. [32]. Fig. 5 shows the influence of the LED wavelength, with maximum emission wavelengths at 386 nm, 392 nm and 397 nm in the 56 LED configuration photocatalytic module, as well as that of the LED number, on the relative evolution of the MEK concentration with time under recirculation over TiO_2 MPT623, for an initial MEK concentration of 20 ppm_v. The Langmuir-Hinshelwood model linear regression derived from experimental degradation data is shown in Fig. 5 and the apparent kinetic rate constants are reported in Table 2. With 56 LEDs, it was worth noting that the 392 nm LEDs yielded the highest MEK degradation, with a complete degradation of MEK within 600 min of time under recirculation, whereas 900 min were necessary using the 397 nm LEDs and more than 1600 min using the 386 nm LEDs. The mineralization was evidenced on the more efficient system by the evolution *vs.* time of the CO_2 concentration, that increased till 70 ppm_v whereas the MEK concentration decreased down to zero, so that the carbon balance was close to 100% after 1500 min of operation. One could note that the CO_2 concentration still increased after complete MEK oxidation occurred, *i.e.* for duration longer than 600 min, as a result from the further oxidation of partially oxidized reaction intermediates (such as acetaldehyde). Although the comparison remained approximate, it was worth noting that the TiO_2 P25/UV-A fluorescence tube-based photoreactor operating at a similar residence time was close to the 386 nm LEDs/TiO_2 MPT623 system in terms of MEK degradation performances, while it remained non-competitive when compared to 392 nm or 397 nm LEDs-based photoreactors.

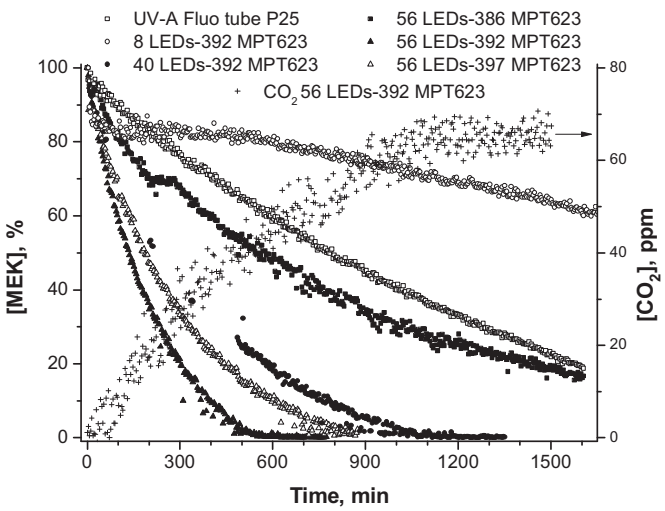

Fig. 5. Influence of the LED wavelength and of the LED number on the relative evolution of the MEK concentration with time under recirculation over TiO_2 MPT623 (9.2 ± 0.2 wt.%)/β-SiC alveolar foam, for an initial MEK concentration of 20 ppm_v. The CO_2 concentration evolution is also reported for the system with 56 LEDs-392 nm. Comparison with results obtained on the TiO_2 P25 (9.0 ± 0.2 wt.%)/β-SiC foam in the UV-A fluorescence tube photoreactor configuration was reported.

Decreasing the number of 392 nm wavelength LEDs led to complete MEK degradation within 600 min and 1200 min, with the 56 LEDs and 40 LEDs device. By contrast, using 8 LEDs was not efficient enough for achieving a complete MEK degradation within more than 4800 min under recirculation, and the 8 LEDs device did not follow a Langmuir–Hinshelwood model, probably due to the presence at the catalyst surface of reaction intermediates in too large amounts that complicates the analysis as usually, so that models taking into account the adsorption competition on the same surface site between MEK and reaction intermediates such as *e.g.* acetaldehyde [23,33] or more generally a multisite kinetic model [30] could by applied for finer analysis. The results globally confirmed that higher the number of LEDs, *i.e.* the light irradiance, higher the MEK degradation efficiency, as was expected.

Among the different tested configurations, the association of 56 LEDs with a maximum emission wavelength at 392 nm to the TiO_2

Table 2
Apparent kinetic rate constant derived from the Langmuir–Hinshelwood model for the different photoreactor configurations and energy effectiveness coefficients calculated for 600 min of use. In case of 392 nm LEDs, an average value of 9.7 mW was taken as input electrical power considering the supplier data in the 8.1 mW (min) – 11.5 mW (max) range.

Number of UV–vis LED392	56			40	8	UV-A Fluo tube
Photocatalyst supported on β-SiC alveolar foam (9.2 ± 0.2 wt.%)	TiO_2 MPT623			TiO_2 MPT623	TiO_2 MPT623	TiO_2 P25 (9.0 ± 0.2 wt.%)
Wavelength (nm)	386	392	397	392	392	365
k (min^{-1})	1.9×10^{-3}	5.2×10^{-3}	3.7×10^{-3}	3.0×10^{-3}	–	9.1×10^{-4}
Energy effectiveness (E_e, mg kW^{-1} h^{-1})	$1.1 \times 10^{+4}$	$2.3 \times 10^{+4}$	$2.6 \times 10^{+4}$	$2.4 \times 10^{+4}$	$3.2 \times 10^{+4}$	$6.3 \times 10^{+2}$

MPT623 photocatalyst led to the highest apparent kinetic rate constant, calculated at 5.2×10^{-3} min^{-1}, and about 6 times higher than that obtained with TiO_2 P25 and a UV-A fluorescent tube, *i.e.* at 9.1×10^{-4} min^{-1}. By contrast, the use of 386 nm and 397 nm LEDs-based systems resulted in a decrease in the apparent rate constant to 1.9 10^{-3} and 3.7 10^{-3} min^{-1}, respectively. Reducing the number of 392 nm LEDs from 56 to 40 resulted in a decrease in the apparent rate constant from 5.2×10^{-3} to 3.0×10^{-3} min^{-1}. So, the results highlighted the interest of associating 392 nm UV/vis LEDs to the TiO_2 MPT623 photocatalyst, in comparison to a standard system based on the TiO_2 P25 reference and a UV-A fluorescent lamp.

Table 2 reports the energy effectiveness coefficients of the different systems, calculated for 600 min of run, which corresponded to the duration of use necessary for reaching a complete MEK removal with the most efficient system, *i.e.* that associating 56 LEDs at 392 nm with TiO_2 MPT623. It was worth noting that energy effectiveness coefficients of LEDs-based systems were about two orders of magnitude greater than that of the UV-A fluorescence tube-based system, being in the range of 10^{+4} mg kW^{-1} h^{-1} *vs.* 10^{+2} mg kW^{-1} h^{-1} for the 365 nm UV-A lighting. Using 56 LEDs, the higher energy effectiveness coefficient was obtained for the 397 nm LEDs-based systems, at $2.6 \times 10^{+4}$ mg kW^{-1} h^{-1}. However, despite greater energy effectiveness, this configuration suffered from weaker removal efficiency when compared to its analogous system based on 392 nm LEDs, being more efficient and displaying an energy effectiveness coefficient of $2.3 \times 10^{+4}$ mg kW^{-1} h^{-1}. In the case of the 392 nm LED system, decreasing the number of LEDs allowed increasing the energy effectiveness coefficient of the system up to $2.7 \times 10^{+4}$ mg kW^{-1} h^{-1} and $3.2 \times 10^{+4}$ mg kW^{-1} h^{-1} for 40 and 8 LEDs, respectively, but both LEDs-based systems suffered from lower MEK degradation performances, especially when the number of LEDs was decreased down to 8. Therefore, a system using 56 LEDs emitting at 392 nm was considered as a good compromise in terms of MEK degradation efficiency and of energy effectiveness when compared to other LEDs-based alternatives, and were highly promising for saving energy in comparison to traditional UV-A lamps. In a fully different photoreactor configuration, the superiority of a UV LEDs-based photoreactor compared to analog ones based on UV-A or UV-C tubes, was already reported by Shie et al., with an energy effectiveness for Ag/TiO_2 P25 being, in the case toluene degradation, 6.1 and 7.4 times larger than that of UV-A and UV-C, respectively [34], and in the case of formaldehyde degradation, 99 and 131 times larger than that of UV-A and UV-C, respectively [11].

4. Conclusion

LEDs have been used as irradiation light source instead of conventional UV-A fluorescent light tube for designing greener and small-size photocatalytic devices incorporating medium surface area open-cell β-SiC alveolar foams as structured photocatalyst support, aiming at providing air purifying technologies with enhanced energy effectiveness. The results illustrated the interest of using a supporting solid alveolar foam and small-size UV/vis LEDs adapted to the TiO_2 photocatalyst absorption range. Taking MEK degradation as gas phase test reaction, associating widespread UV/vis LEDs to a visible-light responsive TiO_2 MPT623 photocatalyst immobilized on β-SiC alveolar foams improved the energy effectiveness of the systems by a factor of about 50 when compared to that of a TiO_2 P25/UV-A system, so that it could be considered as a valuable alternative in the search for efficient and energy saving technologies. Using TiO_2 MPT623 as photocatalyst, a system incorporating 56 LEDs emitting at 392 nm was a good compromise in terms of MEK degradation efficiency and of energy effectiveness.

Acknowledgments

Drs. C. Pham and P. Nguyen from SICAT Catalyst are thanked for providing β-SiC alveolar foams. French ANRT and CIFRE program are thanked for financial support.

Appendix A. Supplementary data

Supplementary data associated with this article can be found, in the online version, at http://dx.doi.org/10.1016/j.apcatb.2014.02.036.

References

[1] S. Romero-Vargas Castrillon, H.I. de Lasa, Industrial & Engineering Chemistry Research 46 (2007) 5867.
[2] D.F. Ollis, H. Al-Ekabi, Photocatalytic Purification and Treatment of Water and Air, Elsevier, Amsterdam, 1993.
[3] P. Pichat, Chemical Degradation Methods for Wastes and Pollutants, in: M.A. Tarr (Ed.), Environmental and Industrial applications, Marcel Dekker Inc., New York, Basel, 2003, pp. 77–119.
[4] N.J. Peill, M.R. Hoffmann, Environmental Science and Technology 30 (1996) 2806.
[5] R.E. Marinangeli, D.F. Ollis, AIChE Journal 26 (6) (1980) 1000.
[6] J.T. Carneiro, R. Berger, J.A. Moulijn, G. Mul, Catalysis Today 147 (1) (2009) S324.
[7] P. Du, J.T. Carneiro, J.A. Moulijn, G. Mul, Applied Catalysis A: General 334 (2008) 119.
[8] H.F. Lin, K.T. Valsaraj, Journal of Applied Electrochemistry 35 (2005) 699.
[9] W.Y. Wang, Y. Ku, Water Research 40 (2006) 2249.
[10] H.W. Chen, Y. Ku, A. Irawan, Chemosphere 69 (2007) 184.
[11] J.L. Shie, C.H. Lee, C.S. Chiou, C.T. Chang, C.C. Chang, C.Y. Chang, Journal of Hazardous Materials 155 (2008) 164.
[12] A.A. Lapkin, V.M. Boddu, G.N. Aliev, B. Goller, S. Polisski, D. Kovalev, Chemical Engineering Journal 136 (2008) 331.
[13] J.P. Ghosh, C.H. Langford, G. Achari, Journal of Physical Chemistry A 112 (2008) 10310.
[14] J.P. Ghosh, R. Sui, C.H. Langford, G. Achari, C.P.A Berlinguette, Water Research 43 (2009) 4499.
[15] Y. Liu, J. Liu, Y. Lin, Y. Zhang, Y. Wei, Ceramics International 35 (2009) 3061.
[16] D.P. Subagio, M. Srinivasan, M. Lim, T.T. Lim, Applied Catalysis B: Environmental 95 (3–4) (2011) 414.
[17] S. Josset, S. Hajiesmaili, D. Begin, D. Edouard, C. Pham-Huu, M.C. Lett, N. Keller, V. Keller, Journal of Hazardous Materials 175 (2010) 372.

[18] S. Hajiesmaili, S. Josset, D. Begin, C. Pham-Huu, N. Keller, V. Keller, Applied Catalysis A: General 382 (1) (2010) 122.
[19] A.N. Kouamé, D. Robert, V. Keller, N. Keller, C. Pham, P. Nguyen, Catalysis Today 161 (1) (2011) 3.
[20] A.N. Kouamé, D. Robert, N. Keller, V. Keller, C. Pham, P. Nguyen, Environmental Science and Pollution Research 19 (2012) 3727.
[21] N. Keller, D. Robert, V. Keller, Immobilisation of a semiconductor photocatalyst on solid supports: methods, materials and applications, in: P. Pichat (Ed.), Photocatalysis and Water Purification: From Fundamentals to Recent Applications, Wiley-VCH, Weinheim, 2013, pp. 145–178.
[22] A.N. Kouamé, R. Masson, D. Robert, N. Keller, V. Keller, Catalysis Today 209 (2013) 13.
[23] G. Vincent, A. Queffeulou, P.M. Marquaire, O. Zahraa, Journal of Photochemistry and Photobiology A: Chemistry 191 (2007) 42.
[24] H. Yu, H. Irie, Y. Shimodaira, Y. Hosogi, Y. Kuroda, M. Miyauchi, K. Hashimoto, Journal of Physical Chemistry C 114 (2010) 16481.
[25] M. Nishikawa, H. Sakamoto, Y. Nosaka, Journal of Physical Chemistry A 116 (2012) 9674.
[26] S. Dai, Y. Wu, T. Sakai, Z. Du, H. Sakai, M. Abe, Nanoscale Research Letters 5 (2010) 1829.
[27] P. Nguyen, C. Pham, Applied Catalysis A: General 391 (1–2) (2011) 443.
[28] T.T. Huu, M. Lacroix, C. Pham Huu, D. Schweich, D. Edouard, Chemical Engineering Science 64 (24) (2009) 5131.
[29] J. Cunningham, G. Al-Sayyed, S. Srijaranai, in: G.R. Helz, R.G. Zepp, D.G. Crosby (Eds.), Aquatic and Surface Photochemistry, Lewis, Boca Raton, FL, 1994, pp. 317–348.
[30] C. Minero, V. Maurino, D. Vione, in: P. Pichat (Ed.), Photocatalysis and water purification, Wiley-VCH, Weinheim, 2013, pp. 53–72.
[31] http://www.comsol.fr/
[32] B. Kartheuser, N. Costarramone, T. Pigot, S. Lacombe, Environmental Science and Pollution Research 19 (2012) 3763.
[33] M.A. Fox, M.T. Dulay, Chemical Reviews 93 (1993) 341.
[34] J.L. Shie, C.Y. Pai, Indoor and Built Environment 19 (5) (2010) 503.